# Wideband Electromagnetic Induction for Metal-Target Identification: Theory, Measurement and Signal Processing

Norbert Geng, Phil Garber, Leslie Collins and Lawrence Carin
Department of Electrical and Computer Engineering
Duke University
Box 90291
Durham, NC 27708-0291

David Hansen, Dean Keiswetter, and I.J. Won
Geophex Ltd.
605 Mercury Street
Raleigh, NC 27603-2343

**Keywords:** mine characterization, modeling, electromagnetic induction, frequency domain, detection, identification, signal processing.

## ABSTRACT

A principal problem with traditional, narrowband EMI sensors involves target identification. As a consequence, in minefield or unexploded ordinance (UXO) detection, for example, each piece of buried metal must be excavated, causing significant false alarms in regions littered with anthropic clutter. Therefore, the principal challenge for the next generation of EMI sensors is development of electronics and algorithms which afford discrimination. To this end, in this paper we operate in the frequency domain, considering wideband excitation and utilize the complex, frequency-dependent EMI target response as a signature.

To test the signature variability of different metal types and target shapes, as well as for calibration of an actual sensor, we have developed a full-wave model for the analysis of wideband EMI interaction with highly (but not perfectly) conducting and permeable targets. In particular, we consider targets which can be characterized as a body of revolution, or BOR. The numerical algorithm is tested through use of a new wideband EMI sensor, called the GEM-3. It is demonstrated that the agreement between measurements and theory is quite good.

Finally, we consider development of signal processing algorithms for the detection and identification of buried conducting and permeable targets, using wideband data. The algorithms are described and then tested on data measured using the GEM-3, with results presented in the form of contour plots as a function of the number of discrete frequencies employed.

## 1. INTRODUCTION

A significant problem with traditional, narrowband electromagnetic induction (EMI) sensors involves target identification. Such sensors have been shown to provide excellent detection of conducting and/or permeable targets, however discrimination between targets and anthropic clutter has proven to be much more difficult[1-7]. As a consequence, in applications such as mine or unexploded ordnance (UXO) detection, each piece of buried metal must be excavated, substantially increasing both the cost and time required to remediate contaminated sites[8]. Therefore, the principal challenge for the next generation of EMI sensors is the development of electronics and algorithms that can afford discrimination, not just detection.

In order to achieve the goal of discrimination, researchers have considered several modifications to the traditional EMI sensor design as well as modifications to the data processing algorithms. One approach has been to recognize that the late-time fields scattered from a conducting and/or permeable target are characterized by an exponential decay in the time domain, similar to that observed from an RL circuit[4-7]. It has been suggested that this decay rate may be useful for target identification, because it is a function of the conductivity, permeability, and shape of the target[4-7]. A second approach has

Part of the SPIE Conference on Detection and Remediation Technologies for Mines and Minelike Targets III
Orlando, Florida • April 1998
SPIE Vol. 3392 • 0277-786X/98/$10.00

been to operate the sensor in the frequency domain, where the differences between the signatures of various targets have also been noted[9]. In this paper, we also operate in the frequency domain, and thus consider wideband excitation. Instead of attempting to extract a decay constant from measured data using a parametric algorithm[10,11], we utilize the complex frequency dependent EMI target response as a signature.

To evaluate target signatures as a function of metal type and shape, we have developed a full-wave model for the analysis of wideband EMI interaction with a class of three-dimensional highly (but not perfectly) conduction and permeable targets. In particular, we consider targets which can be characterized as a body of revolution (BOR). Such targets are rotationally symmetric about at least one axis[12], which is characteristic of many man-made objects. The scattered fields which are due to a current-loop source are calculated using an integral equation formulation which is solved via the Method of Moments (MoM)[13]. The calculations are performed for targets located in free space, and are compared with measurements performed for targets in free space and buried in soil, allowing us to investigate the effects of soil effects over the frequencies of interest. The numerical algorithm is tested through the use of a prototype wideband EMI sensor, called the GEM-3[14]. The GEM-3 can be programmed to transmit waveforms at several discrete frequencies and record the complex target response that is measured at each.

We will show that the agreement between the theoretical calculations and the measured data is quite good. In addition, we show that different targets often have significantly different wideband EMI signatures. These results motivated a detection study, in which signal processing algorithms for the detection and identification of such targets were developed. Results from these analyses are also presented which indicate improved performance (reduced false alarm rate for a fixed detection rate) as a function of the number of discrete frequencies that are incorporated into the detector.

## 2. NUMERICAL MODEL

A frequency-domain boundary-integral equation formulation is used to solve for the fields induced by a highly conducting and/or permeable target in free space due to EMI excitation at kilohertz frequencies. Targets are modeled as a body of revolution (GOR) in order to make such an analysis tractable. The problem is formulated in terms of the tangential electric $\boldsymbol{E}$ and magnetic $\boldsymbol{H}$ fields on the target surface, or, equivalently, in terms of electric and magnetic surface currents, $\boldsymbol{J}=\boldsymbol{n}\times\boldsymbol{H}$ and $\boldsymbol{K}=\boldsymbol{E}\times\boldsymbol{n}$, where $\boldsymbol{n}$ is the outward unit normal. If $\boldsymbol{E}_1$ and $\boldsymbol{H}_1$ represent the electric and magnetic fields inside the target, respectively, $\boldsymbol{E}_2$ and $\boldsymbol{H}_2$ represent the fields outside the target, $\boldsymbol{E}^i$ and $\boldsymbol{H}^i$ represent the incident fields, then the boundary conditions at the interface yield the relationships

$$\boldsymbol{n}\times[\,L_1^{EJ}(-\boldsymbol{J})+L_1^{EK}(-\boldsymbol{K})]=\boldsymbol{n}\times[\,L_2^{EJ}(\boldsymbol{J})+L_2^{EK}(\boldsymbol{K})]+\boldsymbol{n}\times\boldsymbol{E}^i$$

$$\boldsymbol{n}\times[\,L_1^{EJ}(-\boldsymbol{J})+L_1^{EK}(-\boldsymbol{K})]=\boldsymbol{n}\times[\,L_2^{EJ}(\boldsymbol{J})+L_2^{EK}(\boldsymbol{K})]+\boldsymbol{n}\times\boldsymbol{H}^i$$

The operators $L_n$ involve well-known manipulations of the homogeneous-media Green's function[15-17]. The problem therefore reduces to solving for $\boldsymbol{J}$ and $\boldsymbol{K}$, for particular incident fields $\boldsymbol{E}^i$ and $\boldsymbol{H}^i$. The interested reader is referred to[12, 15-18] for details concerning implementation of the general MoM algorithm.

For EMI applications, current-loop excitation is generally used, as opposed to plane-wave fields considered for radar problems. The incident fields are derived from the vector potential[19, 20]

$$A_\phi(\rho,z)\approx\frac{\mu_0 Ia}{4\pi}\int_0^{2\pi}\frac{d\phi'\cos\phi'}{\sqrt{\rho^2+a^2+z-2a\rho\cos\phi'}}$$

Where the origin of the local cylindrical coordinate system $(\rho,\phi,z)$ is situated at the lop center, with axis parallel to z, and I and a are the loop current and radius, respectively. This expression requires a quasi-static approximation since, at the wavelengths in air and soil, the electrical distance between the sensor and target is infinitesimal. The incident electric and magnetic fields are readily computed as

$$H_\rho^i(\rho,z)=-\frac{1}{\mu}\frac{\partial A_\phi}{\partial z},\quad H_z^i(\rho,z)=-\frac{1}{\mu\rho}\frac{\partial(\rho A_\phi)}{\partial\rho},\quad E_\phi^i(\rho,z)=-j\omega A_\phi$$

and these fields are finally expressed in terms of complete elliptical integrals. These fields can be applied directly to the BOR MoM solution if the loop axis and the BOR axis are aligned, and only the lowest order Fourier-series mode is excited (reflecting azimuthal symmetry). If the axes are not aligned, a Fourier-series representation of the incident tangential fields is usually required.

It is also important to note that the EMI fields induced by a conducting and/or ferrous target are generally measured in the near zone, thus the simplifying far-zone approximation generally used for radar problems is not valid[12, 15, 19]. Therefore, the EMI scattered fields are calculated via a rigorous convolution of the calculated currents $\boldsymbol{J}$ and $\boldsymbol{K}$ with the free-space Green's function ($L_2$). In addition, an actual EMI sensor measures the electromotive force induced on a sensing current loop as opposed to the induced fields. To calculate this force, the magnetic field components are integrated over the aperture of the sensing loop to generate a theoretical induced voltage for each target and frequency of interest.

## 3. THEORETICAL AND EXPERIMENTAL RESULTS

In this section, measurements gathered with the GEM-3[14] are compared to predictions from the experimental model. The GEM-3 measures the real and imaginary parts of the voltage induced on the sensing loop, relative to that on the transmitting loop. After multiplying the ratio by $10^6$, the results are reported in units of "parts-per-million", or ppm. In order to compare the theoretical and experimental results, the system must be calibrated at each frequency. To do this, the complex response from a particular target is measured at N orientations, represented as $\mathbf{M}=\{m_1, m_2, \ldots m_N\}^T$, where each $m_i$ is a complex number, and T denotes vector transpose. The theoretical, or calculated, results are represented as $\mathbf{C}=\{c_1, c_2, \ldots c_N\}^T$. The complex calibration constant as a function of frequency, $K(\omega)$ is defined by $\mathbf{MK}=\mathbf{C}$, and the solution for this can be obtained via least squares as $K=(\mathbf{M}^H\mathbf{M})^{-1}(\mathbf{M}^H\mathbf{C})$, where H represents the matrix Hermetian operation.

The agreement that was found between theory and experiment will be demonstrated with a series of examples. In the initial example, a comparison is presented using the data with which the calibration was performed, and which therefore provides an example of the best possible agreement possible between theory and calibrated experimental data. In particular, the target was a brass cylinder of 5.08 cm diameter and 2.34 cm height, situated in free space. Measurements were made with the sensor approximately aligned with the axis of the BOR target at various sensor-target distances. Magnitude and phase results are plotted in Figure 1 for sensor-target distances of 15.24, 20.32, 25.4, and 30.48 cm at six frequencies between 4 and 24 kHz. As expected, the agreement between theory and experiment is quite good, although there is some small disagreement in the phase response.

To test the robustness of the sensor calibration, additional targets were analyzed using the original calibration coefficients $K(\omega)$. The same sensor-target distances as described previously were used. Figure 2 presents results for an aluminum disk of 5.08 cm diameter and 0.3175 cm height. The agreement in the amplitude is very good, while the agreement in phase is respectable, but not as accurate. One explanation of this phenomenon is that the current version of the GEM-3 may have difficulty accurately measuring phase when the amplitude is small.

In general, a strong frequency dependence can be observed in the response waveforms, which can potentially be exploited in detector design. It can be shown that the skin depth ($\delta$) is small relative to the characteristic target dimensions for the targets and frequencies considered here, and it varies as a function of frequency. Therefore, to achieve a strong frequency dependence in the target signature, it is imperative that the operating frequency of the sensor be chosen to coincide with the frequency variation in $\delta$. It is important to note that $\delta$ should not be too small, because at this point highly conducting targets appear to be perfect conductors, and the differences in target conductivities cannot be exploited. Thus, the appropriate operating frequency range is strongly dependent on the targets of interest.

In addition to the strong frequency dependence of the signatures, another consistent feature of the results is the significant variation in the target signature as a function of the sensor-target distance. This feature results from the substantial spatial variation in the excitation fields generated by the GEM-3[14]. This effect renders matched-filter type detectors inappropriate, since in practice the depth of the target is not known. Fortunately, in many applications the statistical distribution of the target depths may be known, and this information can be exploited in designing a detection algorithm[21].

## 4. DETECTOR DESIGN AND EXAMPLE

Based on the results described above, the exploitation of the frequency-dependence of the fields excited by buried conducting and/or permeable targets were investigated in the context of a detector. A test statistic for a frequency-domain EMI sensor was designed, and its performance was evaluated using data measured with the GEM-3. The data used as input to the test statistic, or detector, was the vector $\boldsymbol{m}$ of *calibrated* measured data for the M frequencies utilized

$$\boldsymbol{m} = \{R_1, I_1, R_2, I_2, \ldots\ldots R_M, I_M)^T$$

where $R_1$ is the real part and $I_1$ is the imaginary part of the complex response at the first frequency. A binary hypothesis test is used with $H_0$ representing the "no target", or clutter, hypothesis and $H_1$ representing the target hypothesis. It is further assumed that the measured sensor response, $\boldsymbol{r}$, is subject to additive Gaussian noise, so that $\boldsymbol{r} = \boldsymbol{m} + \boldsymbol{n}$. To effect the likelihood ratio test, which is the optimal solution to a binary hypothesis problem, we must determine $p_{r/H_1}(r/H_1, m, \theta)$, which is the probability density function describing the sensor response $\boldsymbol{r}$ under the target hypothesis given $\boldsymbol{m}$. This density function is also a function of the generalized parameter(s) $\theta$, which have an associated density function $p_\theta(\theta)$. Examples of such parameters include the target-sensor distance and the target orientation. In addition, the probability density function for $\boldsymbol{r}$ under $H_0$, $p_{r/H_0}(r/H_0)$, is also required. Using classical detection theory[22], the optimal test statistic, or likelihood ratio test, is

$$\frac{\int p_{r/H_1}(r/H_1, m, \theta) p_\theta(\theta) d\theta}{p_{r/H_0}(r/H_0)} \underset{H_0}{\overset{H_1}{\gtrless}} T$$

where T is a threshold. As T is varied, the probability of detection and probability of false alarm is adjusted, and the receiver operating characteristic (ROC) is generated. The numerator of the likelihood ratio test provides a mechanism for incorporating the theory described in Section 2 with the detector design by modeling the $\theta$ dependence of $\boldsymbol{m}$. The incorporation of such a model is discussed elsewhere[21], here a suboptimal form of the likelihood ratio which is based on empirical data is used.

The modified likelihood ratio test is implemented by assuming that under $H_0$ the elements are jointly Gaussian with zero means and covariance matrix $K=E\{\boldsymbol{m}\boldsymbol{m}^T\}$, and that under $H_1$ the elements are uniformly distributed. Other distributions have been considered under $H_1$, however the performance is relatively insensitive to the exact form of the density function. The covariance matrix is computed using training data for the environment under test in the absence of targets. To evaluate the validity of this approach, we considered data measured using the GEM-3 at the McKinley Range at Redstone Arsenal. The test site was littered with 100-155 mm projectiles, various other buried munitions, and roofing nails. The targets were buried at a variety of depths, however this was not considered in this analysis. A total of 21 man-made targets were emplaced.

Data was collected by walking the GEM-3 over the site. Dead reckoning was used for navigation. Data was collected at four frequencies, 2.34, 4.05, 7.29, and 12.27 kHz. The modified form of the test statistic was applied to each frequency separately, to combinations of two frequencies, and to all four frequencies simultaneously. Contour plots of the raw data (real and imaginary components) for two of the measured frequencies are shown in Figure 3, where the light gray circles denote the location of emplaced targets. Clearly, an algorithms which simply applies a threshold to the raw contour data cannot locate all of the emplaced targets. Contour plots of the output of the modified detector are shown in Figure 4 for each set of two frequencies (left most and center plots) and for all four frequencies (right-most plot). A substantial improvement is witnessed over the standard thresholding approach, and performance improves with the increase in the number of frequencies used.

One concern regarding this approach is their robustness. A similar statistical algorithm has been applied to land-mine data collected in the presence of significant anthropic clutter under a program sponsored by the US Defense Advanced Research Projects Administration (DARPA)[23]. In those studies, two GEM-3 frequencies were considered. The results, described elsewhere[24], again demonstrated the significant performance gain manifested by fusing the data from multiple

frequencies. However, as noted in Section 2, the frequency range over which such improvements can be obtained is target-class dependent and must be tuned to the problem of interest.

## 5. CONCLUSIONS

We have described a comprehensive study on the potential for wideband EMI to detect and discriminate highly (but not perfectly) conducting and/or permeable targets. A full-wave MoM analysis has been used to model the underlying physics of EMI interaction with a class of targets that can be described as BORs. This analysis indicated that the principal cause of frequency-dependent variation in a target's EMI signature is variation in the skin depth when such is less than the characteristic target dimensions. In this regime, the frequency dependence of the target signature affords the potential for discrimination. The analysis also indicated that the effects of soil can be ignored for buried targets, and this result was confirmed with measured data.

Based on the theoretical results, a detector was designed and the GEM-3 was used to perform a detection study for a US Army test site. The statistical detection algorithm clearly demonstrated that performance improved as the number of frequencies used increased, up to the four that were considered in this study. The density functions used in the derivation of the detector were based on empirical data. In other studies, we have more rigorously implemented the statistical detector[21, 24, 25].

## 6. ACKNOWLEDGEMENTS

This research was sponsored by the Army Research Office under grant DAAH04-96-1-0448 (Demining MURI).

## 7. REFERENCES

1. Das, Y., J.E. McFee, and R.H. Cherry, *Time-domain response of a sphere in the field of a coil: Theory and experiment.* IEEE Trans. Geoscience Remote Sensing, 1984. GE-22: p. 360-367.
2. Das, Y., J. McFee, and G. Stuart, *Analysis of an electromagnetic induction detector for real-time location of buried objects.* IEEE Trans. Geoscience and Remote Sensing, 1990. 28: p. 278-287.
3. Das, Y. and J.E. McFee, *A simple analysis of the electromagnetic response of buried conducting objects.* IEEE Trans. Geoscience Remote Sensing, 1991. GE-29: p. 342-344.
4. Baum, C.E., *Low Frequency Near-Field Magnetic Scattering from Highly, but Not Perfectly Conducting Bodies.* Phillips Laboratory Interaction Note 499, 1993. November.
5. Baum, C.E., N. Geng, and L. Carin, *Integral Equations and Polarizability for Magnetic Singularity Identification.* Phillips Laboratory Interaction Note 524, 1997. March.
6. Geng, N., C. Baum, and L. Carin, *On the low-frequency natural response of conducting and permeable targets.* IEEE Trans. Geoscience and Remote Sensing, 1998. submitted.
7. Sower, S.D. and S.P. Cave. *Detection and Identification of Mines from Natural Magnetic and Electromagnetic Resonances*. in *SPIE*. 1995. Orlando, FL.
8. Dubey, A.C., I. Cindrich, and J.M. Ralston. *Detection Technologies for Mines and Minelike Targets*. in *SPIE*. 1995. Orlando, FL.
9. Trang, A.H., P.V. Czipott, and D.A. Waldron. *Characterization of small metallic objects and non-metallic anti-personnel mines*. in *SPIE*. 1997. Orlando, FL.
10. Van Blaricum, M.L. and R. Mittra, *A Technique for Extracting the Poles and Residues of a System Directly form Its Transient Response.* IEEE Trans. Ant. and Prop., 1975. 23: p. 777-781.
11. Hua, Y. and T.K. Sarkar, *Matrix Pencil Method for Estimating Parameters of Exponentially Damped/Undamped Sinusoids in Noise.* IEEE Trans. Acoust. Speech and Signal Proc., 1990. 38: p. 814-824.
12. Mautz, J.R. and R.F. Harrington, *Radiation and Scattering from Bodies of Revolution.* Appl. Sci. Res., 1969. 20: p. 405-435.
13. Harrington, R.F., *Field Computation by Moment Methods*. 1968, New York: The MacMillan Company.
14. Won, I.J., D.A. Keiswetter, and D.R. Hansen, *GEM-3: A Monostatic Broadband Electromagnetic Induction Sensor.* J. Envir. Engin. Geophysics, 1997. 2: p. 53-64.
15. Mautz, J.R. and R.F. Harrington, *Electromagnetic Scattering from a Homogeneous Material Body of Revolution.* AEU, 1979. 33: p. 71-80.

16. Glisson, A.W. and D.R. Wilton, *Simple and Efficient Numerical Methods for Problems of Electromagnetic Radiation and Scattering from Surfaces.* IEEE Trans. Ant. and Prop., 1980. 28: p. 593-603.
17. Glisson, A.W., D. Kajfez, and J. James, *Evaluation of Modes in Dielectric Resonators Using Surface Integral Equation Formulation.* IEEE Trans. Microwave Theory Tech., 1983. 31: p. 1023-1029.
18. Wu, T. and L.L. Tsai, *Scattering from Arbitrarily Shaped Lossy Dielectric Bodies of Revolution.* Radio Science, 1977. 12: p. 709-718.
19. Balanis, C.A., *Advanced Engineering Electromagnetics*. 1989, New York: John Wiley and Sons.
20. Simonyi, K., *Theoretische Elektrotechnik*. 1980, Berlin: VEB Deutscher Verlag der Wissenschaften.
21. Gao, P. and L. Collins. *Improved signal processing approaches for landmine detection.* in *SPIE*. 1998. Orlando, FL.
22. Van Trees, H.L., *Detection, Estimation, and Modulation Theory*. 1968, New York: John Wiley and Sons.
23. George, V., *et al.*, *Background Data Collection Plan*, . 1996, DARPA/Defense Science Office.
24. Collins, L., P. Gao, and L. Carin, *An Improved Bayesian Decision Theoretic Approach for Land Mine Detection.* IEEE Trans. Geosc. Remote Sens., 1997. submitted.
25. Gao, P. and L. Collins, *A 2-Dimensional Generalized Likelihood Ratio Test for Land Mine Detection.* Signal Processing Letters, 1998. submitted.

**Figure 1a - Measured and computed voltage (magnitude) induced by electromagnetic induction interaction with a brass cylinder of 5.08 cm diameter and 2.34 cm height, situated in "free space". Solid curves: measured, dashed: theory.**

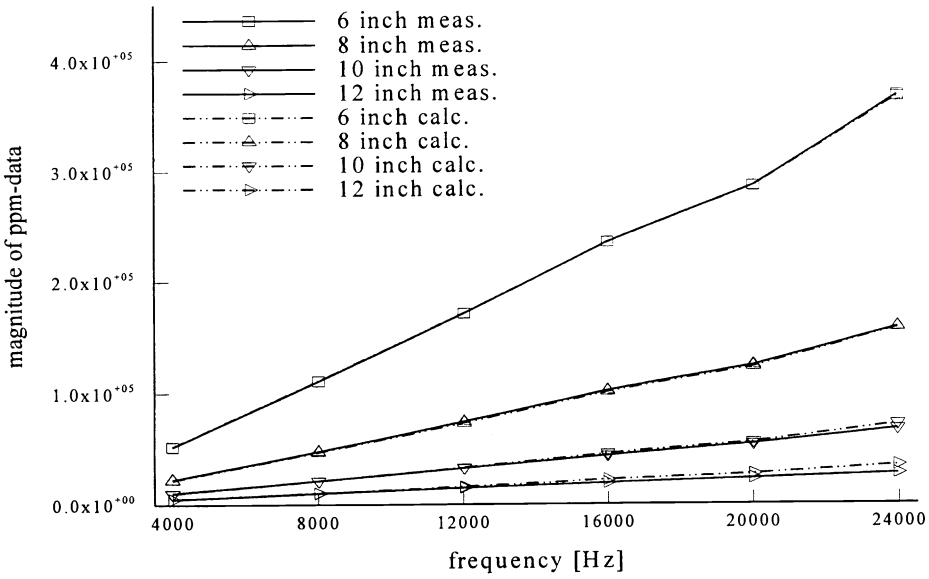


**Figure 1b - Measured and computed voltage (phase) induced by electromagnetic induction interaction with a brass cylinder of 5.08 cm diameter and 2.34 cm height, situated in "free space". Solid curves: measured, dashed: theory.**

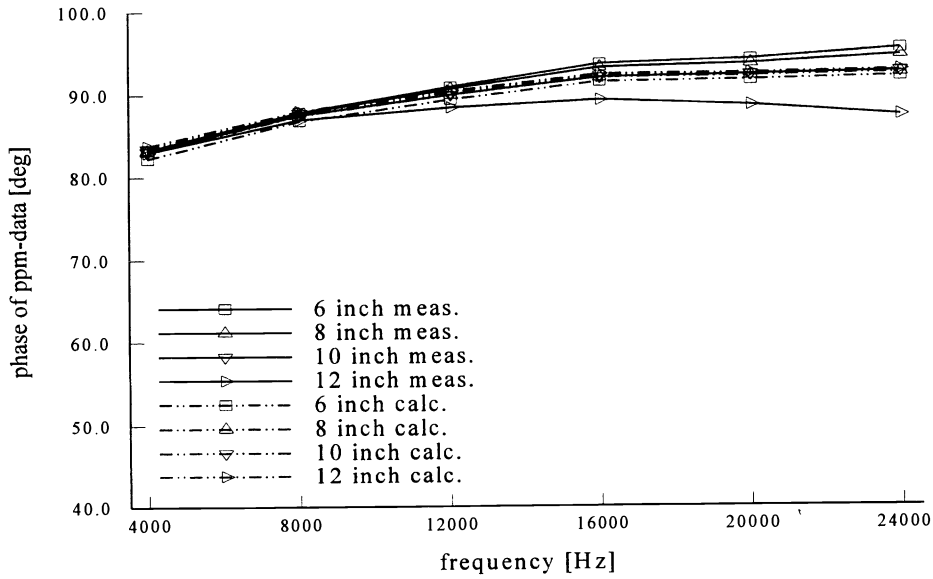

**Figure 2a: As in Figure 1, for an aluminum disk of 5.08 cm diameter and 0.635 cm height (magnitude).**

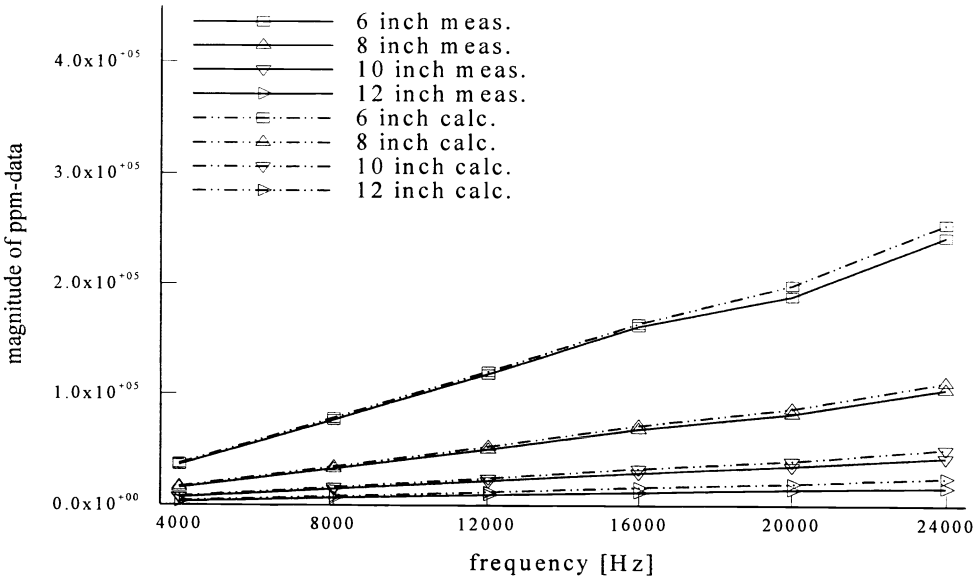


**Figure 2b: As in Figure 1, for an aluminum disk of 5.08 cm diameter and 0.635 cm height (phase).**

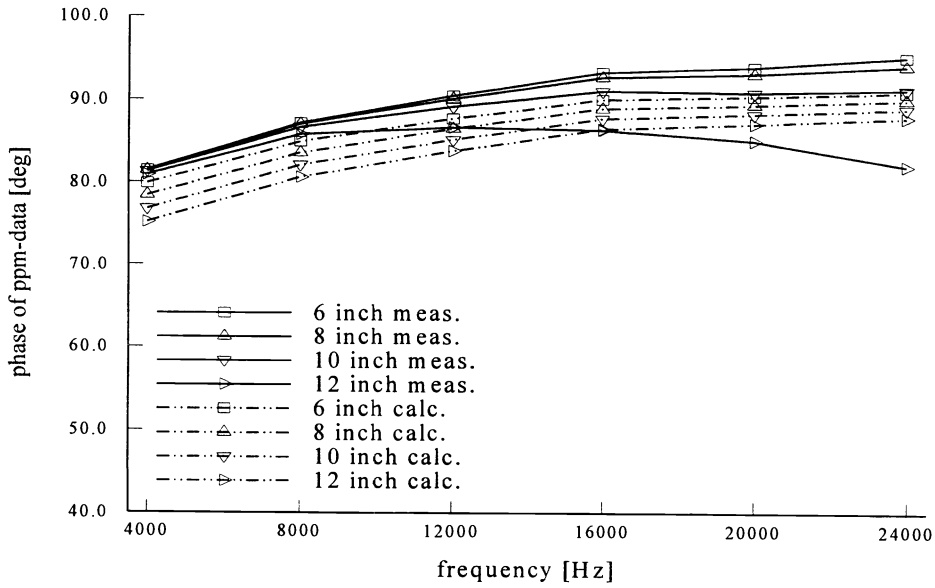

**Figure 3. Contour plots of real and imaginary data for two of the four measured frequencies. Gray circles denote locations of emplaced targets.**

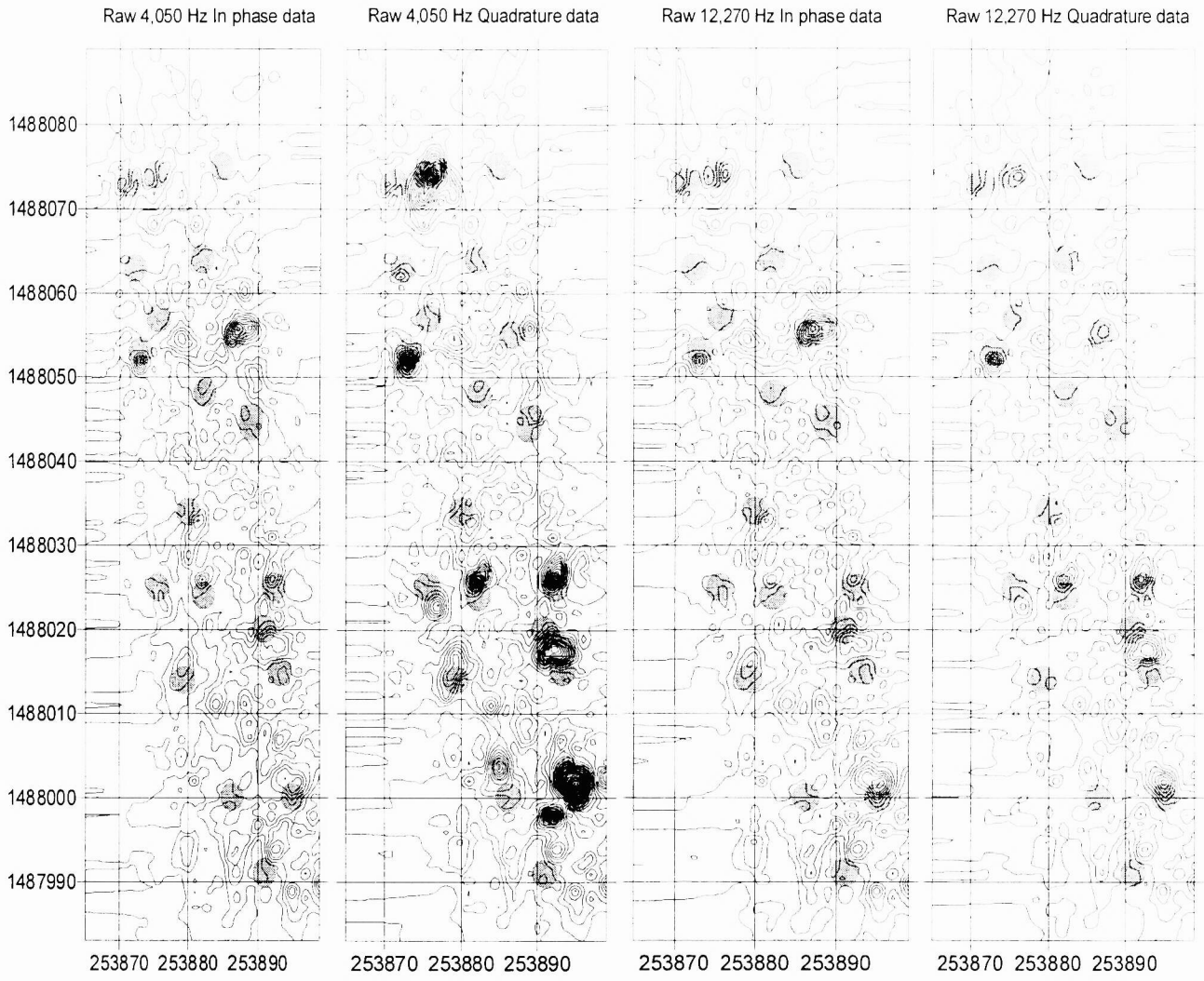

**Figure 4. Contour plots of output of statistical detector using first two frequencies (left), second two frequencies (middle), and all four frequencies (right). Gray circles denote locations of emplaced targets.**